The molecular architecture of hemidesmosomes as revealed by super-resolution microscopy

Leila Nahidiazar[1], Maaike Kreft[1], Bram van den Broek[1], Pablo Secades[1], Erik M. M. Manders[2], Arnoud Sonnenberg[1,*], and Kees Jalink[1,*]

[1]Division of Cell Biology, The Netherlands Cancer Institute, Plesmanlaan 121, 1066 CX Amsterdam, The Netherlands

[2]Van Leeuwenhoek Centre for Advanced Microscopy, Swammerdam Institute for Life Sciences, University of Amsterdam, Amsterdam, The Netherlands

* Authors for correspondence: Arnoud Sonnenberg (a.sonnenberg@nki.nl) or Kees Jalink (k.jalink@nki.nl)

Summary

Hemidesmosomes have been extensively studied by immunofluorescence microscopy, but due to its limited resolution, their precise organization remained poorly understood. We studied hemidesmosome organization in cultured keratinocytes by 2- and 3-color super-resolution microscopy. We observed that in the cell periphery, nascent hemidesmosomes are associated with individual keratin filaments and that β4 is distributed along rather than under keratin filaments. By applying innovative methods to quantify molecular distances, we demonstrate that the hemidesmosomal plaque protein plectin interacts simultaneously and asymmetrically with β4 and keratin. Furthermore, we show that BP180 and BP230 are characteristically arranged within hemidesmosomes with BP180 surrounding a central core of BP230 molecules. In skin cross-sections, hemidesmosomes of variable sizes could be distinguished with BP230 and plectin occupying a position in between β4 and BP180, and the IF system. In conclusion, our data provide a detailed view of the molecular architecture of hemidesmosomes in cultured keratinocytes and skin.

Introduction

Classical type I hemidesmosomes (HDs) are rivet-like structures, which play a critical role in maintaining tissue integrity and resisting mechanical force (Walko et al., 2015). At the ultrastructural level, they appear as electron-dense plaques present on the cytoplasmic side of the plasma membrane to which keratin intermediate filaments (IF) are anchored. At the core of each HD is the integrin α6β4, a receptor for laminin-332 in the epidermal basement membrane that binds to the intermediate filament (IF) anchoring protein plectin (Borradori and Sonnenberg, 1999). Two other components of type I HDs are the Bullous Pemphigoid antigens BP180 (collagen type XVII or BPAG2) and BP230 (BPAG1e). A second type of HD (type II HD), present in simple epithelia and many cultured cells, lacks the BP antigens; it contains only plectin and α6β4 (Litjens et al., 2006).

A model for the spatial organization of HD components has been proposed in which the two transmembrane proteins α6β4 and BP180 are connected via plectin and BP230 to the IF system (Koster et al., 2003, 2004). However, it is not known how the different HD components are spatially organized relative to one another. Neither is it known how the keratin-IFs are anchored to HDs in cultured keratinocytes or whether they are directly involved in the organization of the HD structure (Song et al., 2015; Seltmann et al., 2015).

Here we have used two- and three-color Ground State Depletion followed by Individual Molecule return microscopy (GSDIM) (Hell, 2007) and quantitative image analysis to characterize in detail the architecture of nascent HD in cultured keratinocytes. Additionally, we have applied GSDIM in the study of HDs in tissue sections of human skin.

Results and Discussion

Plectin and β4 are localized alongside keratin filaments

Studies on the role of keratin filaments in the organization of HDs at the periphery of keratinocytes, where the assembly of filaments is initiated, have been hampered by the limited resolution of immunofluorescence microscopy. SR microscopy of human keratinocytes revealed that the keratin-14 organization at the cell periphery differs significantly from that in the more central parts (supplementary material Fig. S1A). While thick keratin filament bundles occur in the center of the cell, an elaborate network of fine keratin filaments running close and parallel to the basal membrane is present at the cell periphery.

To visualize keratin filaments together with either plectin or β4, we optimized imaging conditions and introduced precise correction algorithms for acquisition of two or three very high quality color channels from the same cell (see M&M and supplementary material Fig. S1B,C). The results show that β4, detected with a mAb against its extracellular domain, is closely associated with keratin filaments. But rather than overlapping, β4 is found along the keratin filaments that run parallel to the plasma membrane (Fig. 1A). In line with the notion that keratin filaments loop through HD plaques, they do not stop at sites where β4 is present, but rather connect these molecules while extending farther into the cytoplasm and along the plasma membrane.

Quantification of the spatial relationship between these two proteins by conventional co-localization analysis, using e.g. Pearson or Manders coefficients cannot be applied to the high SR resolution images. We therefore developed alternative measures and Image J software routines to quantify protein-protein proximity at the nanometer scale (Fig. 1A, supplementary material Fig. S2). We determined the distribution of orthogonal distances between β4 and keratin-14 by first manually delineating single keratin filaments. Regions of interest (ROI) containing these filaments were cut to smaller images, and the delineated filaments (splines) with associated β4 were straightened by affine transformation, a procedure which preserves molecular distances (Fig. supplementary material S2). The graph in Fig. 1A shows the distribution of distances between β4 and the filament present in 120 ROIs. This analysis revealed that most β4 is indeed distributed alongside, rather than under the

keratin filaments, with an average distance of 68±8 nm to the axis of the keratin filament (Fig. 1A, supplementary material Fig. S3). In contrast, a β4 mutant (β4^{R1281W}) that is unable to bind to plectin (Geerts et al., 1999), is found to be equally distributed under and along keratin filaments (Fig. 1B, supplementary material Fig. S4).

We next visualized the localization of the cytolinker plectin using a mAb against the central rod domain. Like β4, plectin is co-distributed with keratin filaments (Fig. 1C) and excluded, at least partially, from the area immediately under the filaments. The mean distance between the rod domain of plectin and keratin filament (Fig. 1C, graph) was smaller than that between the extracellular domain of β4 and keratin filaments (56±6 nm versus 68±8 nm). In the cells expressing β4^{R1281W}, the rod domain of plectin appeared to be more closely localized to the keratin filaments (supplementary material Fig. S4), indicating that the distance between plectin and the keratin filaments is influenced by its binding to β4. As expected, an antibody directed against the plectin C-terminus localized closer to keratin, as witnessed from the overlap in the distance distributions (Fig. 1D, supplementary material Fig. S3). Three-color SR imaging for keratin-14, β4 and plectin confirms that β4 and plectin are co-distributed with keratin filaments (Fig. 1D).

These findings provide the first direct microscopical confirmation that plectin interacts simultaneously and asymmetrically with β4 and keratin; i.e. the N-terminus binds to β4 while the C-terminus associates with keratin (Geerts et al., 1999; Nikolic et al., 1996). Furthermore, they underscore the importance of keratin filaments in orchestrating the assembly of HDs (Seltmann et al., 2013).

Distribution of BP230 and BP180 in HDs

Next, we examined the spatial distribution of BP180 and BP230 by SR microscopy and proximity analysis. A close association between the C-terminus of BP230 and keratin-14 was observed in SR images (Fig. 2A). In contrast, BP180, detected with an antibody against its extracellular domain, was located farther from the keratin filaments. It displayed a wider, bimodal distribution with a typical distance of about 56 nm (Fig. 2B). This distance is less than that between the cytoplasmic domain of β4 and keratin (68 nm, see Fig. 1A), perhaps reflecting the difference in size between

plectin and BP230. Together, these observations corroborate the notion that BP230 binds keratin via its C-terminus.

Imaging of immunolabeled BP180 and BP230 together revealed a remarkable pattern of the distribution of the two molecules. BP230 is often observed to form bright punctae which are almost invariably surrounded by BP180 molecules, seemingly at a regular and characteristic distance (Fig. 2C). This is particularly apparent in areas where the molecules are relatively sparse (Fig. 2C), whereas in more dense regions BP180 labeling becomes somewhat continuous in stripes that appear to follow the filaments (data not shown). Analyses of (radial) distance distributions in sparse regions (Fig. S2) indicated an average distance of 55 nm between BP180 and the center of the BP230 punctae. In summary, our data indicate that BP180 and BP230 are assembled into highly organized concentric structures distinct from those of β4 and plectin.

BP180 and BP230 co-distribute with β4 and plectin in HDs

The distribution of BP180 and BP230 relative to β4 and plectin in type I HDs was determined using antibodies against the extracellular domains of both BP180 and β4. The results show that in the stripe-like structures that are co-distributed with keratin filaments (Fig. 1 and 2) the two transmembrane proteins are in close proximity of each other (Fig. 3A). More towards the periphery of the cell, there is a region in which β4 occurs without labeling of BP180, while at the very front of the cell some isolated BP180 proteins are present. BP230 and plectin, detected with antibodies against their C-terminals appear closer to each other, in line with their direct interaction with keratin filaments (Fig. 3B).

To quantitatively support these observations, we developed an automatic image analysis method for mapping protein proximity in SR images (Fig. S2C). Molecular proximity is visualized by false-color (blue) superposition, the intensity of which decreases with increasing distance between the red and green labels. In the proximity map of Fig. 3C, the spots with an intense blue color indicate that BP180 and β4 are not distributed mutually exclusively but rather are localized together in large parts of the cell. No specific proximity was detected between β4 and an unrelated membrane protein, MHC Class 1 heavy chain (not shown). In these analyses, proximity cut-off was set at 70 nm. Importantly, there is no tight association

between the two molecules in the outermost region of the cell periphery (Fig. 3D). Proximity mapping of BP230 and plectin (Fig. 3E) yielded a narrower blue-striped structure, indicating their presence in close apposition to keratin filaments. The filamentous patterns for the different pairs of HD components in the proximity maps provide further support for a role of keratin in the organization of HDs in cultured keratinocytes (Fig. 2 and 3).

In conclusion, proximity mapping shows that BP180 and β4 are not distributed alternatingly or randomly but concur in large regions of the cells (Fig 3C-E). The data support a model in which nascent HDs, formed at the outer zone of the cell, mature in the more central parts of the cell by recruitment of BP230 and BP180 (Koster et al., 2004).

SR fluorescence microscopy of HD components in skin.

To investigate and compare the molecular organization of HDs in cultured keratinocytes with that in tissues, we performed SR fluorescent microscopy on cross-sections of human skin. Antibodies against the extracellular domain of β4 produced a discontinuous linear staining pattern along the basis of the keratinocytes, whereas antibodies against keratin-14 apparently reacted with an irregular and dense network of keratin filaments in the cytoplasm (Fig. 4A). Strikingly, there is a visible gap of 50-150 nm between the two labels that likely reflects the space occupied by plectin and the intracellular part of β4. The gap was detectably smaller when an antibody against the β4 cytoplasmic domain was used (Fig. 4B). Furthermore, sections labeled with antibodies against the central rod-domain (Fig. 4C) or the C-terminal keratin-binding domain of plectin (not shown) showed tight proximity of keratin and plectin with little, if any, discernible space between them. Staining for BP180 (cytoplasmic domain) and BP230 (C-terminal domain) revealed that in skin sections BP230 is also in close proximity to keratin filaments (Fig. 4D), whereas there is a gap of 100-150 nm between BP180 and keratin (Fig. 4E). We also often found BP230 in distinct punctae at the basal membrane (Fig. 4D,F). These results illustrate that the architecture of HD in skin, with the cytolinkers plectin and BP230 linking keratin filaments to transmembrane proteins β4 and BP180, resembles that observed in cultured keratinocytes.

In summary, we have mapped the position of proteins in HDs in unprecedented detail by SR microscopy and proximity analysis and for the first time convincingly show that in the peripheral parts of the cells, HDs are associated with keratin filaments.

Materials and Methods

Antibodies

The following antibodies were used: anti-keratin-14 (Covance), 121 (rod domain of plectin; Hieda et al.,1992), 233 (cytoplasmic domain of BP180; Nishizawa et al.,1993), 439-9B (extracellular domain of β4), 450-11A (cytoplasmic domain of β4), 5E (C-terminal domain of BP230; Ishiko et al., 1993), P1 (C-terminal plakin-repeat of plectin; Stegh et al., 2000) and anti-BP230 (C-terminal domain of BP230; Tanaka et al., 1990). Secondary goat antibodies were: anti-rat (Alexa 488 or Alexa 647), anti-rabbit (Alexa Fluor 488/Alexa Fluor 532/Alexa Fluor 647), anti-mouse (Alexa Fluor 488/Alexa Fluor 532/Alexa Fluor 647), anti-guinea pig (Alexa Fluor 488) and anti-human (Alexa Fluor 488) from Invitrogen.

Cell lines and immunofluorescent analysis

PA-JEB/β4 and PA-JEB/β4^{R1281W} keratinocytes were cultured as described (Geerts et al., 1999). For immunofluorescent analysis, keratinocytes grown on coverslips were fixed, permeabilized and incubated with primary and secondary antibodies at RT with extensive washing steps in between.

Sections (~5 μm thick) of skin frozen in optimal cutting temperature (OCT) compound were placed on coverslips coated with 10% poly-L-lysine and dried for 1 hour at RT. After washing with PBS for 5 minutes, they were fixed in 2% paraformaldehyde for 10 minutes, blocked with 2% BSA in PBS and incubated with primary and secondary antibodies as described above.

Optimized SR imaging

SR microscopy in TIRF or epi-fluorescence mode was with a Leica SR-GSD microscope (Leica Microsystems) equipped with 488, 532 and 647 nm lasers, using 160x oil immersion objective and, for 3D images, an astigmatic lens. Much effort was dedicated towards optimization of two- and three-color image acquisition as well as to post-acquisition corrections. A full description is given in supplementary material Fig. S1B, C and the legend.

Acknowledgements

Figures
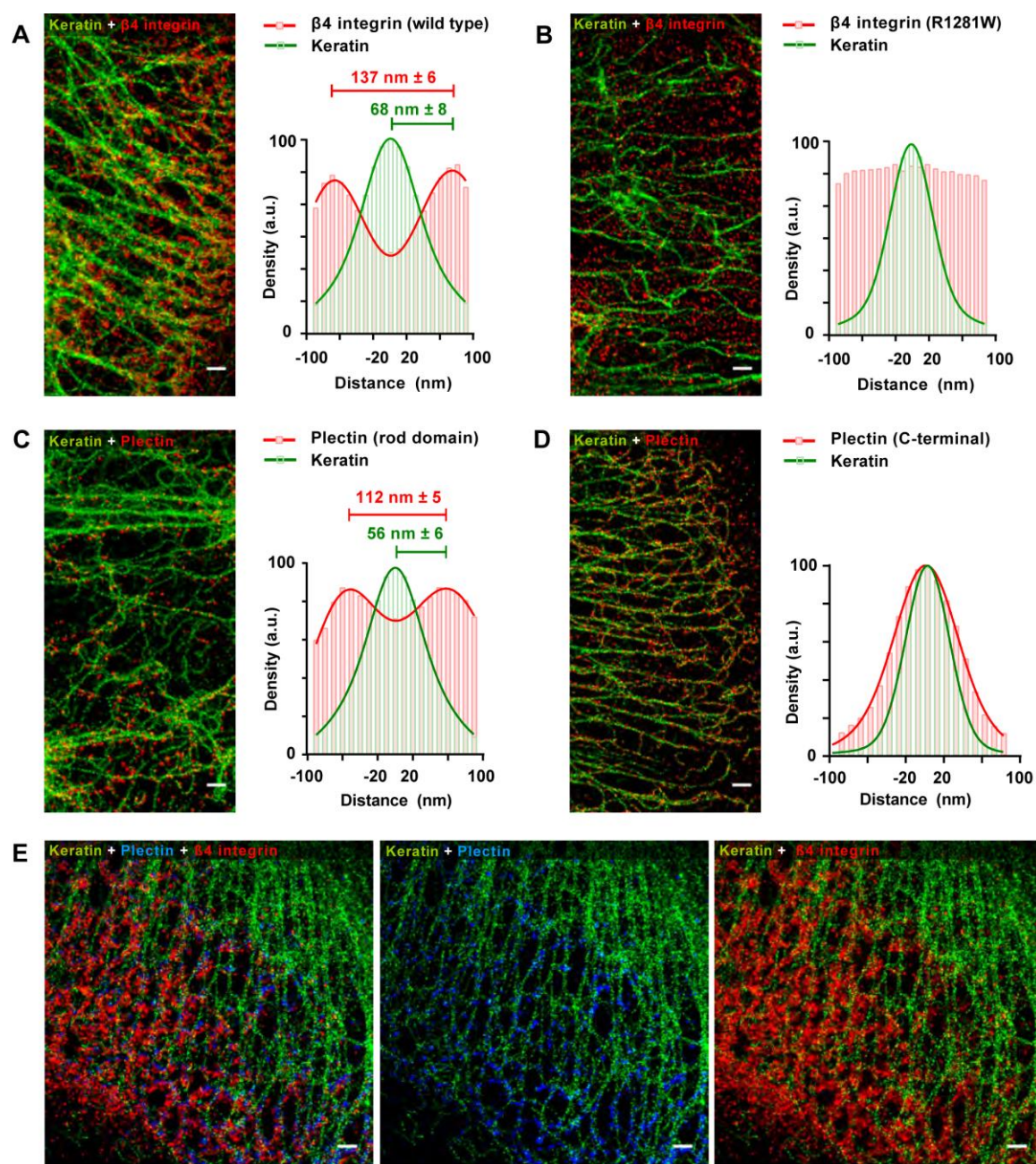
**Fig. 1. SR images of keratin, integrin β4 and plectin in cultured keratinocytes.**

(**A**) SR image of β4 and keratin-14. Graphs show the average distance distribution between β4 and keratin for n=283 ROIs taken from 30 cells (right). Scale bars are 500 nm. Further details on image analysis are presented in supplementary material Fig. S2. (**B**) SR image (left) and distance distribution (right) for keratin and a β4 mutant (β4^{R1281W}) that is unable to bind plectin. Data are averages of 109 ROIs in 10 cells. (**C**) SR image (left) and distance distribution (right) for keratin and plectin (rod domain). Data are averages of 98 ROIs in 10 cells. (**D**) SR image (left) and distance distribution (right) for keratin-14 and the keratin-binding C-terminus of plectin. The overlap in localizations confirms that the plectin C-terminus interacts with keratin. Data are averages from 100 ROIs taken from 15 cells. (**E**) Three-color SR imaging illustrating that plectin (rod domain) and β4 (extracellular domain) decorate keratin filaments in a similar pattern.
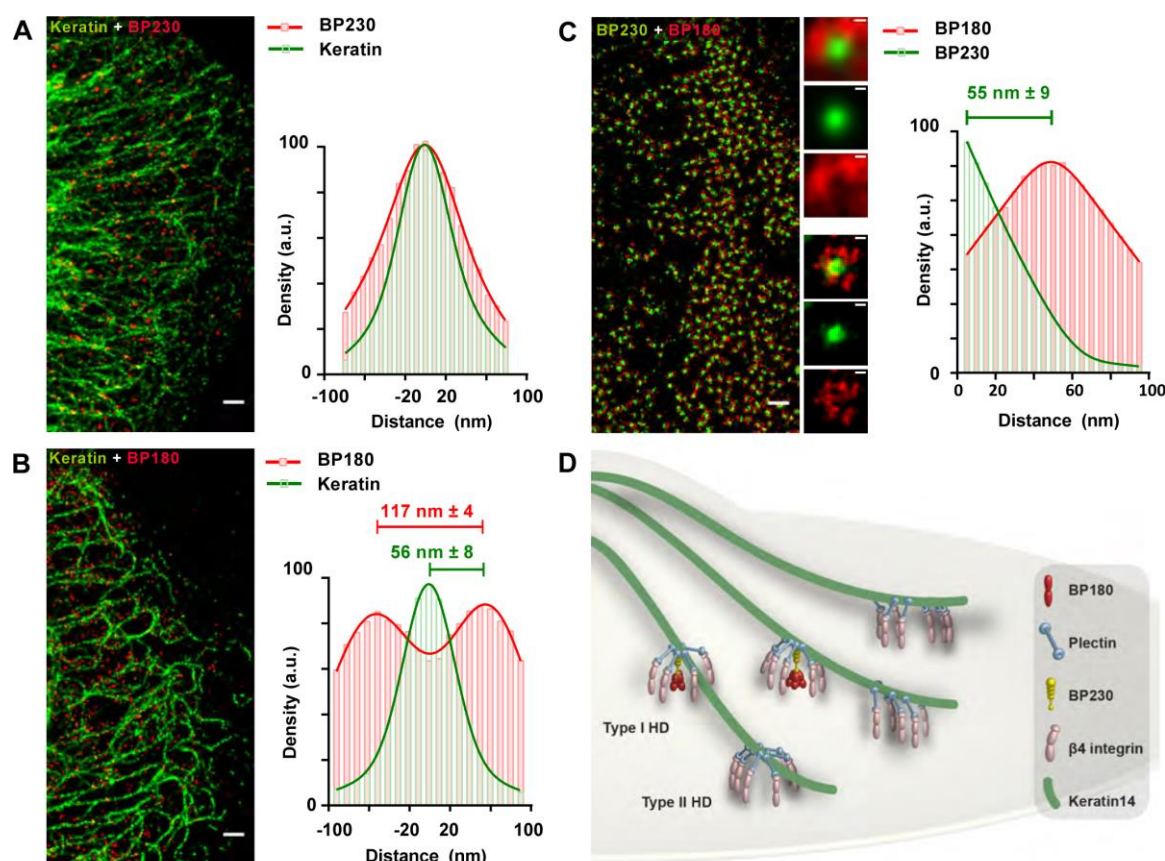
Fig. 2. Keratin, BP230 and BP180 location at super-resolution.

(**A**) SR image of BP230 (IF-binding domain) and keratin-14. The distance distributions of keratin-14 and BP230 show that both labels overlap considerably. Data are from 93 ROIs in 11 cells. Scale bars are 500 nm. (**B**) SR image of BP180 and keratin and distance distribution showing that BP180 is partly present alongside the filaments while significant overlap also occurs. Data are from 172 ROIs in 14 cells. (**C**) SR image of BP230 and BP180 showing dense punctae of BP230 surrounded by BP180. A region with relatively sparse labeling was selected to allow resolving separate complexes. The magnifications (scale bar 100 nm) depict a single type I HD (lower 3 panels) and an average projection of 53 HDs (top 3 panels). For details, see the text and Fig. S2B. Right panel: Distribution of molecular distances between BP180 and BP230. (**D**) Drawing showing 3D model for type I and II HDs. In type I HDs small circular clusters of BP180 molecules are closely linked to keratin filaments via BP230. Integrin β4 is anchored to filaments via plectin in a 'tent-and-peg' model. Type II HDs, formed at the outermost region of the cell, only consist of β4 and plectin.
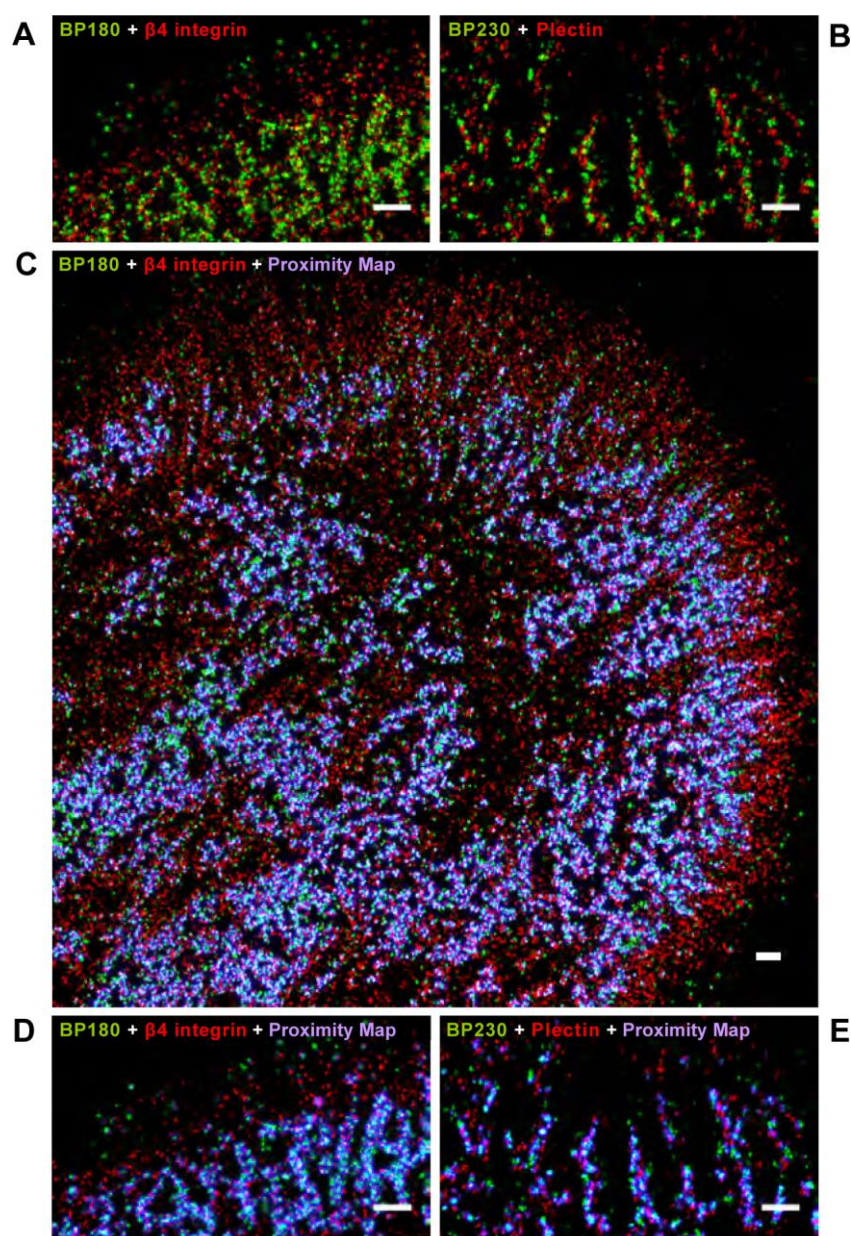
Fig. 3. Proximity mapping of HD components in keratinocytes.

(**A**) In keratinocytes, labeled BP180 and β4 often appear in stripes but also as individual dots. Note the appearance of single BP180 dots at the very edge of the cell and a region with predominant labeling of β4 adjacent to it. Stripe-like structures decorated with both labels are found about 1 μm farther inwards. Scale bars 500 nm. (**B**) Stripe-like localization of BP230 and plectin is visible at some distance from the cell margin but not at the cell edge. (**C**) Proximity map of BP180 and β4. The intensity of the blue color throughout the cell visualizes the prevalence of small molecular distances (< 70 nm) between the two labels. Stripe-like blue areas of close

proximity are not present in the outermost area (~ 1 μm). As in (**B**), single BP180 molecules are present at the outermost region of the cell and β4 occupies a small zone of ~1 μm adjacent to it. Lack of blue coloration shows that the distance between these two molecules is more than 70nm. (**D**, **E**) Detailed proximity maps of the regions depicted in (**A**) and (**C**). Note that the blue bands in (**E**) are slightly narrower than those in panel (**D**), reflecting a shorter distance between the cytolinker protein and keratin filaments. Representative images of 3-5 experiments are shown.
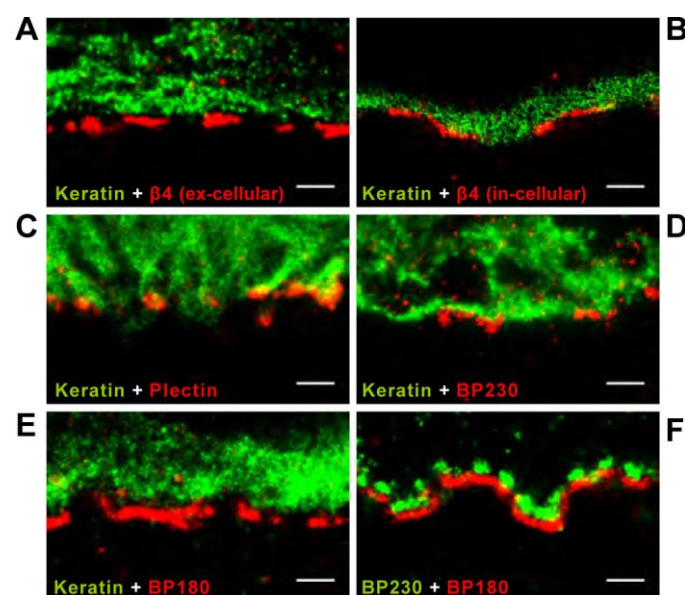
Fig. 4. SR imaging of HD components in human skin sections.

(**A**) Cross section of human skin tissue. The distribution of β4 (extracellular domain) and keratin-14 shows a distinct gap of 50-150 nm, likely reflecting the space occupied by the cytolinker plectin. (**B**) The labels of keratin-14 and the cytoplasmic domain of β4 are juxtaposed but do not overlap. (**C**) Keratin-14 and plectin (rod domain) labels partially overlap and show no visible gap. (**D**) The BP230 label partially overlaps with that of keratin-14 with no discernable gap. (**E**) A gap of about 100-150 nm is also visible between keratin and BP180. (**F**) Individual HDs resolved by SR imaging in human skin. Like *in vitro*, in skin sections BP230 appears punctate and surrounded by patches of BP180. All images are representatives of at least 5 different preparations. Scale bars: 500 nm.

References

Borradori, L. and Sonnenberg, A. (1999). Structure and function of hemidesmosomes: more than simple adhesion complexes. *J. Invest. Dermatol*. **112**, 411-418.

Geerts, D., Fontao, L., Nievers, M.G., Schaapveld, R.Q., Purkis, P.E., Wheeler, G.N., Lane, E.B., Leigh, I.M. and Sonnenberg, A. (1999). Binding of integrin α6β4 to plectin prevents plectin association with F-actin but does not interfere with intermediate filament binding. *J. Cell Biol.* **147**, 417-434.

Hell, S.W. (2007)**.** Far-field optical nanoscopy. *Science* **316**, 1153-1158.

Hieda, Y., Nishizawa, Y., Uematsu, J. and Owaribe, K. (1992). Identification of a new hemidesmosomal protein, HD1: a major, high molecular mass component of isolated hemidesmosomes. *J. Cell Biol.* **116**, 1497-1506.

Ishiko, A., Shimizu, H., Kikuchi, A., Ebihara, T., Hashimoto, T. and Nishikawa, T. (1993). Human autoantibodies against the 230-kD bullous pemphigoid antigen (BPAG1) bind only to the intracellular domain of the hemidesmosome, whereas those against the 180-kD bullous pemphigoid antigen (BPAG2) bind along the plasma membrane of the hemidesmosome in normal human and swine skin. *J. Clin. Invest.* **91**, 1608-1615.

Koster, J., Geerts, D., Favre, B., Borradori, L. and Sonnenberg, A. (2003). Analysis of the interactions between BP180, BP230, plectin and the integrin α6β4 important for hemidesmosome assembly. *J. Cell Sci.* **116**, 387-399.

Koster, J., van Wilpe, S., Kuikman, I., Litjens, S.H. and Sonnenberg, A. (2004). Role of binding of plectin to the integrin β4 subunit in the assembly of hemidesmosomes. *Mol. Biol. Cell* **15**, 1211-1223.

Litjens, S.H., de Pereda, J.M. and Sonnenberg, A. (2006). Current insights into the formation and breakdown of hemidesmosomes. *Trends Cell Biol.* **16**, 376-383.

Nikolic, B., Mac Nulty, E., Mir, B. and Wiche, G. (1996). Basic amino acid residue cluster within nuclear targeting sequence motif is essential for cytoplasmic plectin-vimentin network junctions. *J. Cell Biol.* **134**, 1455-1467.

Nishizawa, Y., Uematsu, J. and Owaribe, K. (1993). HD4, a 180 kDa bullous pemphigoid antigen, is a major transmembrane glycoprotein of the hemidesmosome. *J. Biochem.* **113**, 493-501.

Seltmann, K., Roth, W., Kroger, C., Loschke, F., Lederer, M., Huttelmaier, S. and Magin, T.M. (2013). Keratins mediate localization of hemidesmosomes and repress cell motility. *J. Invest. Dermatol.* **133**, 181-190.

Seltmann, K., Cheng, F., Wiche, G., Eriksson, J.E. and Magin, T. (2015). Keratins stabilize hemidesmosomes through regulation of β4-integrin turnover. *J. Invest. Dermatol.* **135**, 1609-1620.

Song, J.G., Kostan J, Drepper F, Knapp B, de Almeida Ribeiro E Jr, Konarev PV, Grishkovskaya I, Wiche G, Gregor M, Svergun DI, Warscheid B, Djinović-Carugo K. (2015). Structrual insights into Ca2+-calmodulin regulation of plectin 1a-integrin β4 interaction in hemidesmosomes. *Structure.* **23**, 558-570.

Stegh, A.H., Herrmann, H., Lampel, S., Weisenberger, D., Andra, K., Seper, M., Wiche, G., Krammer, P.H. and Peter, M.E. (2000). Identification of the cytolinker plectin as a major early in vivo substrate for caspase 8 during CD95- and tumor necrosis factor receptor-mediated apoptosis. *Mol. Cell Biol.* **20**, 5665-5679.

Tanaka, T., Korman, N.J., Shimizu, H., Eady, R.A., Klaus-Kovtun, V. Cehrs, K. and Stanley, J.R. (1990). Production of rabbit antibodies against the carboxy-terminal epitopes encoded by bullous pemphigoid cDNA. *J. Invest. Dermatol.* **94**, 617-623.

Walko, G., Castañón, M.J. and Wiche, G. (2015). Molecular architecture and function of the hemidesmosome. *Cell Tissue Res*. **360**, 529-544.
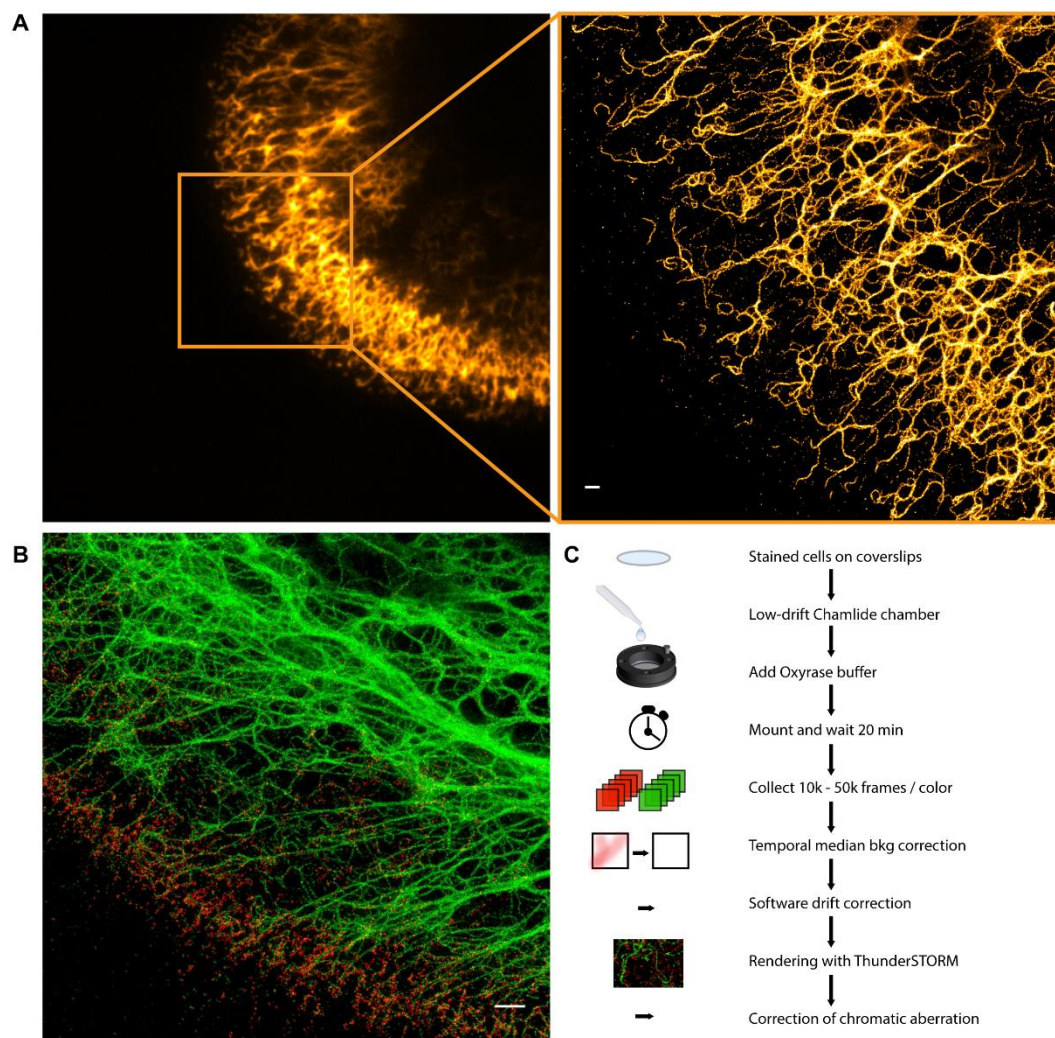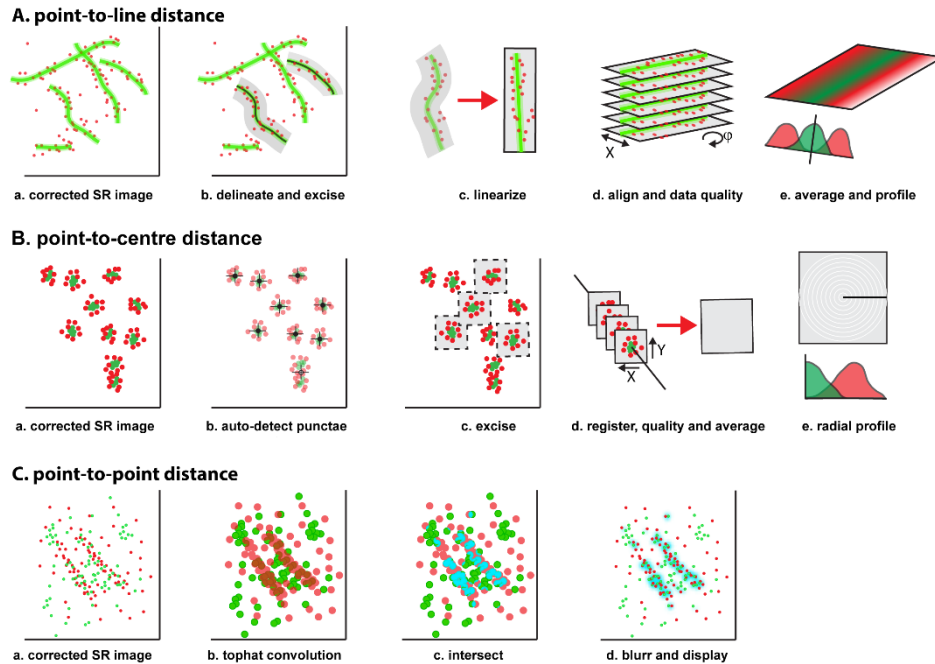
Figure S1. Imaging the fine keratin filament network in the periphery of the cell.
(A) Keratin filaments observed by TIRF (left) and SR microscopy (right). The SR image shows individual filaments running parallel to the basal membrane. The filaments in the outer rim of the cell are thinner in diameter. Scale bar: 500 nm. (B) Optimized two-color SR image of keratin and plectin. Scale bar: 500 nm. (C) Schematic overview of the various optimized acquisition and correction steps to obtain the highly-corrected two- and three-color GSD images in this paper.

Coverslips with stained cells were mounted in a Chamlide CMB magnetic chamber (Live Cell Instrument, Seoul, South Korea). Of several commercial dishes and holders, the Chamlide holders were found to have minimal drift, as detected by analyzing long time-lapse image series taken from coverslips with sparse sub-resolution fluorescent beads (Invitrogen). Popular imaging buffers for SR microscopy are typically optimal only for a single channel (fluorescent dye). Since physicochemical blinking mechanisms may vary widely between different dyes, the fluorophores in extra channels (second- and third colors) show suboptimal blinking kinetics and brightness, leading to significantly diminished image quality in these channels. We tested several alternative buffer formulations, aiming specifically to optimize blinking for two- and three-dye SR imaging and thereby obtain high quality multi-color images.

These tests resulted in a new oxygen scavenging buffer, termed OXEA (a mixture of mercaptoethylamine (50 mM), the oxygen scavenger system Oxyrase (OXYRASE Inc, Mansfield, Ohio, USA, 3%) and sodium-L-lactate (12%, w/w) in PBS). We found that this buffer supports fast and bright blinking of Alexa Fluor-647, AF-488 and AF-532 for two- and three-color imaging (full details to be published elsewhere). After addition of 500 µl of OXEA to the coverslips, cells were mounted on the microscope and the preparation was left to stabilize for 15-30 min to avoid initial drift before SR data were acquired. A total of 10.000 to 50.000 frames (10 ms) were collected for each channel. Blinking detection threshold was set at 70 photons/pixel (~500 photons/event). For 2-color imaging, the Alexa-647 channel was imaged first, followed by Alexa-488. These two dyes show essentially no leak-through. For 3-color SR imaging, we first imaged Alexa-647, followed by Alexa-488 (with 500/30 band-pass filter to prevent leak-through of Alexa-532). Thereafter, Alexa-488 had bleached enough to prevent leak through in the third channel, Alexa-532. For post-acquisition correction steps, data were transferred to an off-line workstation. First, we applied our temporal median background correction (Hoogendoorn et al., Scientific Reports 2014) to the raw data using home-built software (available on request). This correction proved especially powerful to improve the image quality in densely labeled structures. Following that, any residual X/Y drift was removed from the data using a home-built 'de-jittering' routine. For image rendering, the Image J plugin ThunderSTORM (Ovesny et al., Bioinformatics 2014) was used with final pixel size of 10 nm and, if many events were present, additional filtering to reject the least precise localizations. Alternatively, the built-in de-jittering algorithm of recent versions of ThunderSTORM was used. As a final step, chromatic aberrations (CA) were precisely corrected. CA (of up to 60 nm) was mapped throughout the focal plane by imaging 0.1 µm diameter Tetraspec microspheres (Invitrogen) embedded in a matrix. An affine transformation matrix was constructed from those data and affine correction of all images was carried out using a home-build ImageJ macro (available on request). CA was highly stable over several months of imaging. While elaborate, these improvements allowed us to routinely obtain very good quality two- and three-color images.

A. point-to-line distance

a. corrected SR image · b. delineate and excise · c. linearize · d. align and data quality · e. average and profile

B. point-to-centre distance

a. corrected SR image · b. auto-detect punctae · c. excise · d. register, quality and average · e. radial profile

C. point-to-point distance

a. corrected SR image · b. tophat convolution · c. intersect · d. blurr and display

Figure S2. Calculation of molecular distance distributions and proximity mapping.
(A) Determining the distribution of distances between one label decorating a filament and an arbitrary second label. In SR images (a) containing filaments and additional label(s), the centers of individual un-branched filaments was delineated manually by drawing curved lines (b) of 500 nm width onto the keratin channel. We made sure that filaments were single-stranded and well-separated so as to avoid potential overlap with nearby filaments. Then each of the selected curved Regions Of Interest (ROI) surrounding a single filament was excised (b) and linearized (c) using the straightening (affine transformation) routine in ImageJ. This routine warps the image so as to linearize the curved lines as well as the image area surrounding it. Because radius of curvature is very large in relationship to the detected distances, this does not alter the average distances of individual points (β4, etc.) to the linearized filaments. The straightened filaments (ROIs) were precisely oriented vertically by image rotation, divided up in shorter line segments of ~1 μm long and centered laterally with sub-pixel resolution (d) by Gaussian fitting of the intensity profile of the filaments. This automated alignment procedure (macro available on request) corrects for slight inaccuracies in tracing, and it allows for data cleanup by discarding those sub-images in which the Gaussian fit does not fulfill constraints on filament width and goodness-of-fit. To calculate the distribution of distances between keratin and the second color channel (integrin β4, plectin, BP230 or BP180) the sub-images were summed and projected onto a line orthogonal to the filament direction (e). Validity of this analysis was verified by analyzing synthetic (in silico) data sets with our routines. These tests showed that the affine transformation and alignment routines did not affect average measured distances, while only a very slight (~ 1 nm) effect was observed on the width of the distribution. (B) To detect radial distances in the circular patterns of BP230 and BP180 (a), punctae of bright staining were detected by thresholding and size-exclusion based on the BP230 channel (b), and the surrounding regions of interest (200 x 200 nm) (c) were copied into an ROI image dataset. Excised ROIs were automatically aligned with sub-pixel precision based on the center of gravity of the BP230 signal (d), and the average image of all data was constructed for both channels (d, below). The intensity-distance distribution was then made by averaging the intensities in concentric circles with indicated radii to the center of BP230 (e). (C) To produce pixel maps that visualize molecular proximity (at a user-selected scale), the two color channels (a) are convolved with a normalized 2D circular top-hat kernel of size R (b), which evenly dilates individual bright pixels over a range R while keeping the integrated intensity unchanged. On the resulting images conventional colocalization was applied using thresholding according to Costes method (Costes et al., 2004), after which local proximity was computed as (SQRT (gray value$_{channel1}$ x gray value$_{channel 2}$)) (c). This procedure thus yields a proximity map that depicts vicinity of the two colors up to a scale R. This method can be extended to show proximity in a distance r (range $0<r<R$) by subtracting two proximity maps produced with kernel sizes R and r. By overlaying the *proximity map* with the original multicolor Super-Resolution image (d), the places in the image where the two labels are in close vicinity are clearly marked visually. As control, no significant proximity was observed between β4 and an Ab against an unrelated membrane protein, MHC heavy chain. All data analysis was based on the nr of ROIs indicated in the text. ROIs were selected from 7-30 individual cells, and each experiment was carried out at least 5 times on separate days. Further information and software routines may be obtained by emailing k.jalink@nki.nl
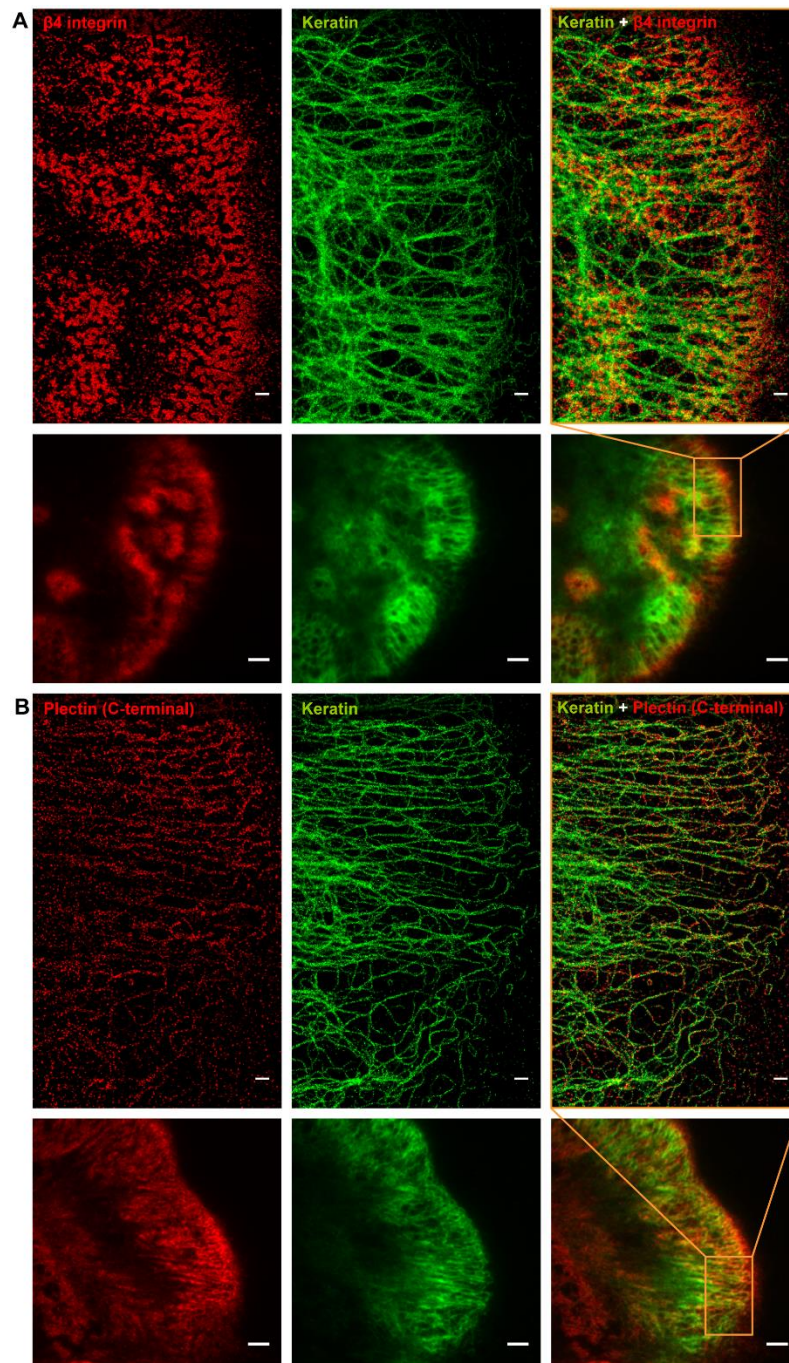
Figure S3. Comparison of the distribution of β4 and plectin with keratin-14 in PA-JEB/β4 keratinocytes.
Representative high-resolution images of cells stained for keratin-14 and β4 integrin (A) or for keratin-14 and plectin (B; Ab against the C-terminus), together with the TIRF images to provide cellular context. Note that the pdf images allow zoom-in to 10 nm resolution. Scale bars are 500 nm (3 μm for TIRF images).
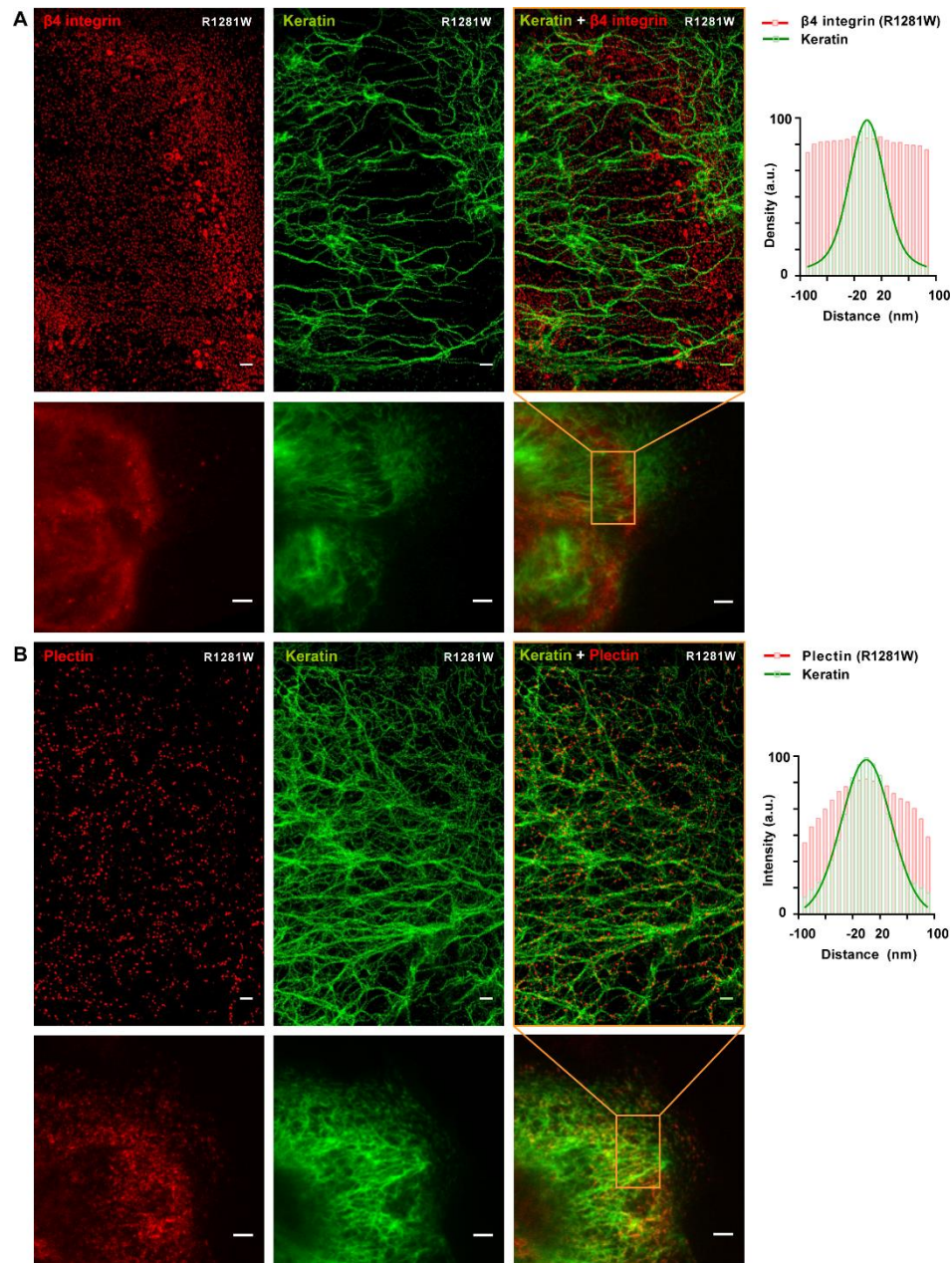
Figure S4. Comparison of the distribution of β4 and plectin with keratin-14 in PA-JEB keratinocytes expressing β4 ^{R1281W}.

(A) High-resolution and TIRF images of cells stained for keratin-14 and β4 integrin. The graph showing the distance distribution between plectin and keratin-14 is identical to that in Fig. 1B. It illustrates that there is no specific distribution of β4 along the keratin filaments in these cells. (B) High-resolution and TIRF images of keratin-14 and plectin (Ab against rod domain). The graphs show the distance distribution between plectin and keratin-14 in PA-JEB keratinocytes expressing mutant β4 ^{R1281W}. Because the β4 mutant cannot interact with plectin, plectin is no longer held in position along keratin filaments but is flexible. The consequent change in distribution from bi-modal (Fig. 2C; wt β4) to unimodal (β4 R1281W) supports the tent-and-peg model. Average results are shown from n=160 ROIs taken from n=8 cells. Scale bars are 500 nm (3 µm for TIRF images).

References:

Costes, S.V., Daelemans, D., Cho, E.H., Dobbin, Z., Pavlakis, G., and Lockett, S. (2004). Automatic and quantitative measurement of protein-protein colocalization in live cells. *Biophys J*. 86, 3993-4003.

Hoogendoorn, E., Crosby, K.C., Leyton-Puig, D., Breedijk, R.M., Jalink, K., Gadella, T.W., and Postma, M. (2014). The fidelity of stochastic single-molecule super-resolution reconstructions critically depends upon robust background estimation. *Sci. Rep*. 4, 3854.

Ovesný, M., Křížek, P., Borkovec, J., Svindrych, Z., and Hagen, G.M. (2014). ThunderSTORM: a comprehensive ImageJ plug-in for PALM and STORM data analysis and super-resolution imaging. *Bioinformatics* 30, 2389-2390.